AE 2610, Lab #04

What Breaks the Wind? Stalling in a Wind Tunnel

By: **Madeleine Graham**

Group A1Y

Fall Semester 2021

Abstract

This experiment measured the forces and moments on a wing with an axisymmetric airfoil at two different windspeeds with and without an endplate at multiple angles of attack in a low-speed wind tunnel. It was found that stall occurred at higher angles of attack with a higher freestream velocity. It was also found that the addition of an endplate significantly increases the coefficient of lift, but also increases the coefficient of drag. An error analysis was performed and results were largely within 3% uncertainty with 95% confidence.

Introduction

The experiment was carried out in the low-speed wind tunnel with a maximum velocity of about 16 m/s. The quantities measured were the gauge pressure inside the test section, the axial and normal forces and pitching moment on the test specimen, and the air density. The static and stagnation pressures were measured with pitot tubes, and the loads were measured with a load cell attached to the specimen. The loads were monitored at angles of attack ranging from 0 to 20 degrees over two different experimental conditions: high vs. low speed, and with or without an endplate. The purpose of this experiment was to observe the effects of high vs. low speeds and endplate vs. no endplate at varying angles of attack on C_l, C_d, and C_m of the wing specimen, which is a finite wing with an axisymmetric airfoil.

Experimental Setup

The wind tunnel used was an open-return type wind tunnel in the Georgia Institute of Technology Montgomery-Knight building. The wind tunnel draws air from the room with a large fan into honeycomb filters, which undo the rotation caused by the fan. The air then goes through a contraction cone so that it will speed up before entering the test section or “working section” (see Figure 1) where the specimen is located.

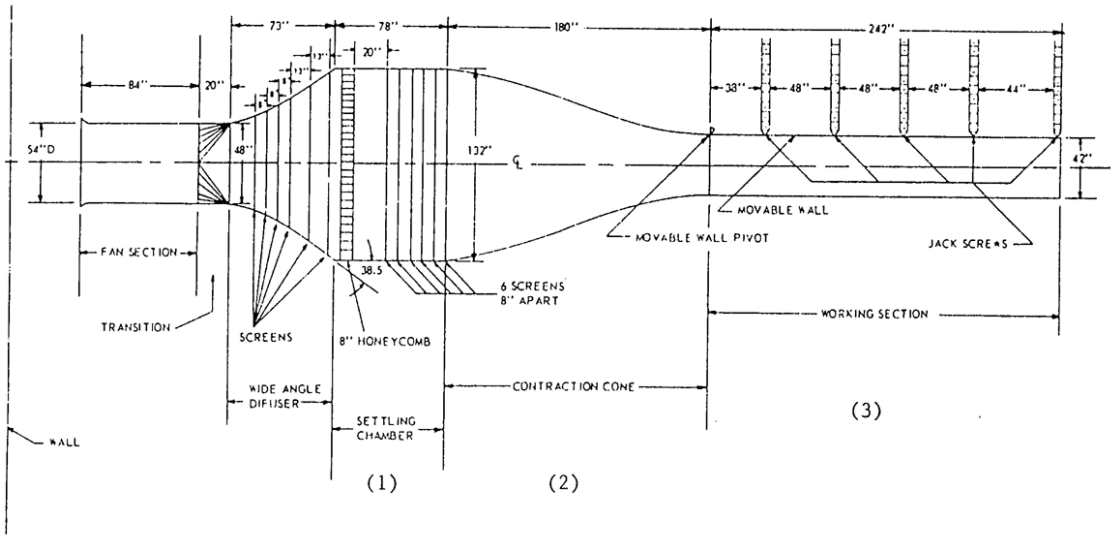

Figure 1: A schematic of the Georgia Tech Low Turbulence Wind Tunnel

A pitot-static probe is in the test chamber and feeds gauge pressure data to the Baratron. For this experiment, a FlowKinetics Manometer/Flow Speed Meter was also connected to the test section for independent verification of pressure and or velocity and to measure the air density (Figure 2).

Figure 2: The FlowKinetics Manometer and its density measurement on the day of the experiment (1.16 kg/m^3)

The test specimen wing was attached to a load cell with a stepper-motor, which was controlled through LabView VI. LabView was used to monitor rough calculations of C_l, C_d, and freestream velocity as well as save the collected data after each experiment. After turning on the wind tunnel, the specimen was manually zeroed using LabView controls so that a C_l of 0 appeared on the display. Then, a preprogrammed sequence was initiated that collected 3 seconds of data for each angle of attack from 0 to 20 degrees.

Results and Discussion

General Data Results and Reduction

The details of the specimen were provided before performing the experiment and are detailed in the following Table I:

Table I: Information about the wing specimen

Dimension	Value (m)	Value (m^2)
Span (wing)	0.686	
Span (endplate)	0.002	
Chord (wing)	0.310	
Chord (endplate)	0.559	
Max Thickness (wing)	0.076	
Max Thickness (endplate)	0.229	
Surface Area (wing)		0.213

The experiment was first carried out at a windspeed of about 16.5 m/s. The windspeed data was calculated using voltage data from the Baratron multiplying it by the relation provided (1.016 mmHg / V), and relating it dynamic pressure using Bernoulli's Equation:

$$p_0 - p = \frac{1}{2}\rho_\infty v_\infty^2 \qquad (1)$$

(Bernoulli's Equation may be used here, because at windspeeds this low, the air is assumed to be incompressible.)

P_0-P is the gauge pressure reading from the Baratron, ρ_∞ is the freestream density calculated, and v_∞ is the freestream velocity. As stated above, air density ρ was measured with the FlowKinetics Manometer and since we are assuming incompressible flow, ρ is assumed constant despite the changing freestream velocities. Windspeed data calculated are in Table II.

Table II: Calculated average windspeed of each experiment

Experiment	Average Windspeed (m/s)
High Speed, with endplate	16.55
High Speed, without endplate	16.54
Low Speed, with endplate	13.57
Low Speed, without endplate	13.06

Since the load cell only measured axial and normal loads on the wing, Lift and Drag forces were measured using trigonometric relations.

$$L = F_y\cos\alpha - F_x\sin\alpha \quad (2)$$

$$D = F_x\cos\alpha + F_y\sin\alpha \quad (3)$$

F_x and F_y are the axial and normal forces on the wing and α is the angle of attack. C_l and C_d were then obtained by non-dimensionalizing Lift and Drag:

$$C_l = \frac{L}{q_\infty S} \quad (4)$$

$$C_d = \frac{D}{q_\infty S} \quad (5)$$

$$C_m = \frac{M}{q_\infty Sc} \quad (6)$$

q_∞ is dynamic pressure, which is the same as the value measured by the Baratron using the relation in Eq 1. S is the planform area, and c is the chord length (Table I). M is the pitching moment measured by the load cell.

Endplate Discussion

By plotting C_l vs. α we obtain Figures 3 and 4, which illustrate that the coefficient of lift is higher at nearly all angles of attack with the endplate present in both the higher and lower freestream velocity conditions.

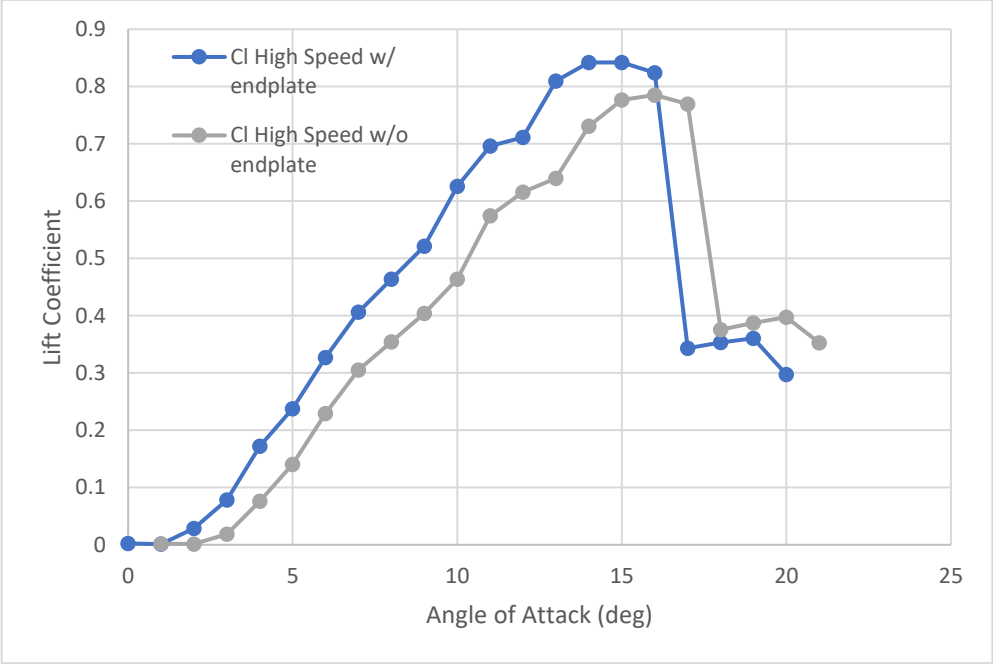

Figure 3: C_l vs. α at ~16 m/s with and without the endplate

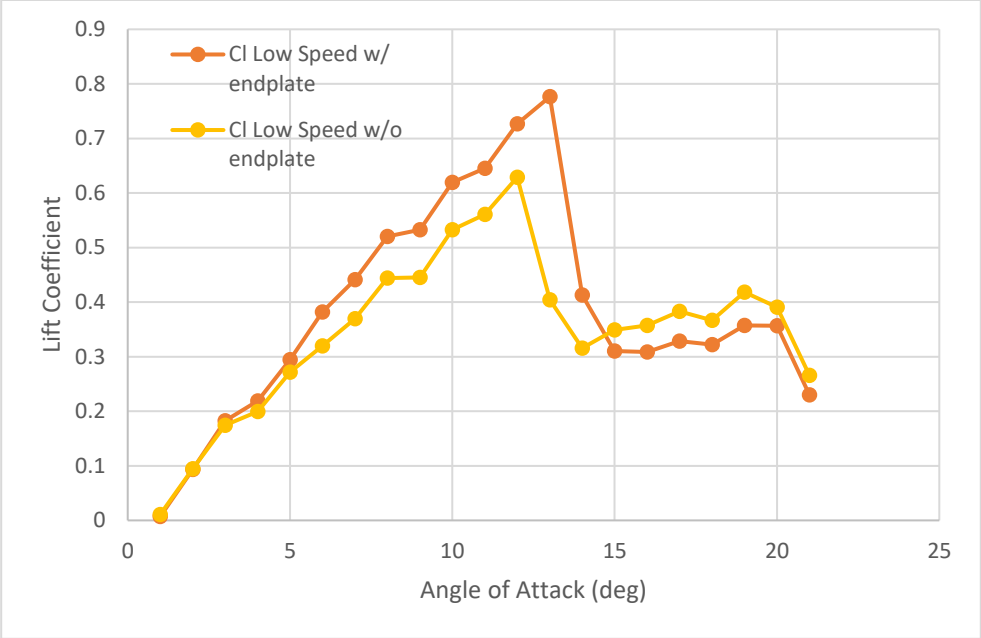

Figure 4: C_l vs. α at ~13 m/s with and without endplate

These trends may indicate that the notion of downwash, which is caused by wingtip vortices creating essentially a downward component of airflow, influences the coefficient of lift. The endplate halts flow over the wing from curling around the sides, creating these vortices, and thus stymies the effect of downwash. Therefore, the higher coefficient of lift coinciding with an endplate attached to the wing is well within expectations.

Figures 5 and 6 show a picture that is not quite as clear. At higher speeds (Figure 5), C_d is lower without an endplate than with an endplate. At lower speeds (Figure 6), C_d is about the same with or without the endplate attached.

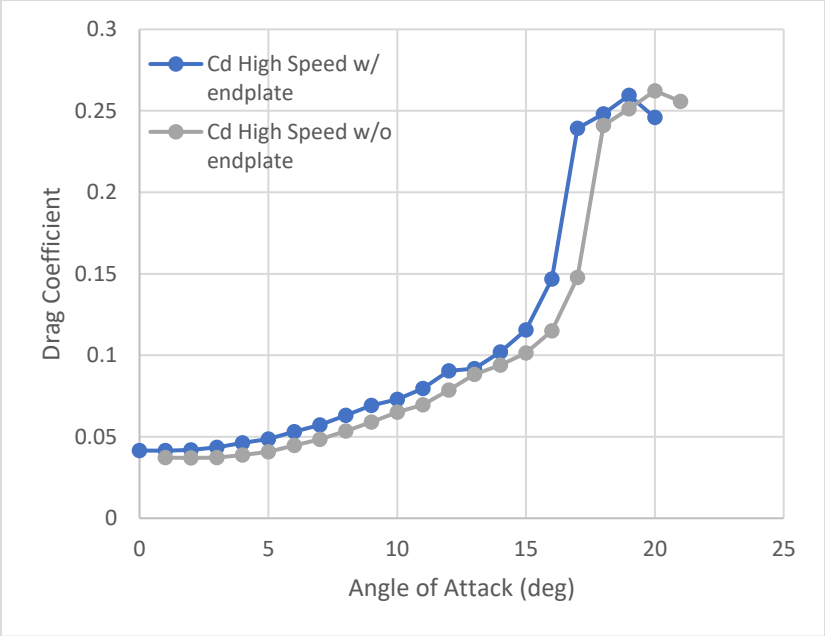

Figure 5: C_d vs. α at ~16 m/s with and without an endplate

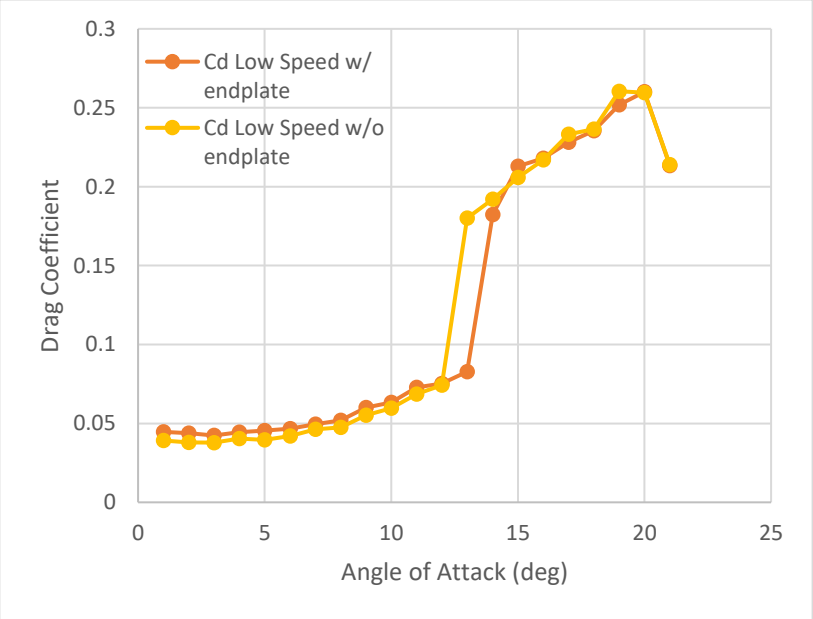

Figure 6: C_d vs α at ~13 m/s with and without endplate.

This seems to contraindicate the results from before, where C_l was higher due to the presence of the endplate. The effect of downwash should be that the drag coefficient, C_d is higher without the endplate. Perhaps the presence of the endplate creates more drag than it staves off. Another

possibility is that the effect of induced drag is accounted for in the way that Lift is calculated. Lift is calculated as the normal component to the freestream velocity (see Equation 2). A downward force would resolve as reduction of Lift, and not the addition of Drag. Therefore, the effect of downwash or reduction of downwash by the presence of the endplate cannot be seen here: only the drag created by the extra friction present as a result of the endplate can be seen.

Figure 7 shows how there is about a maximum 0.1 difference between C_l and C_d at higher freestream velocity.

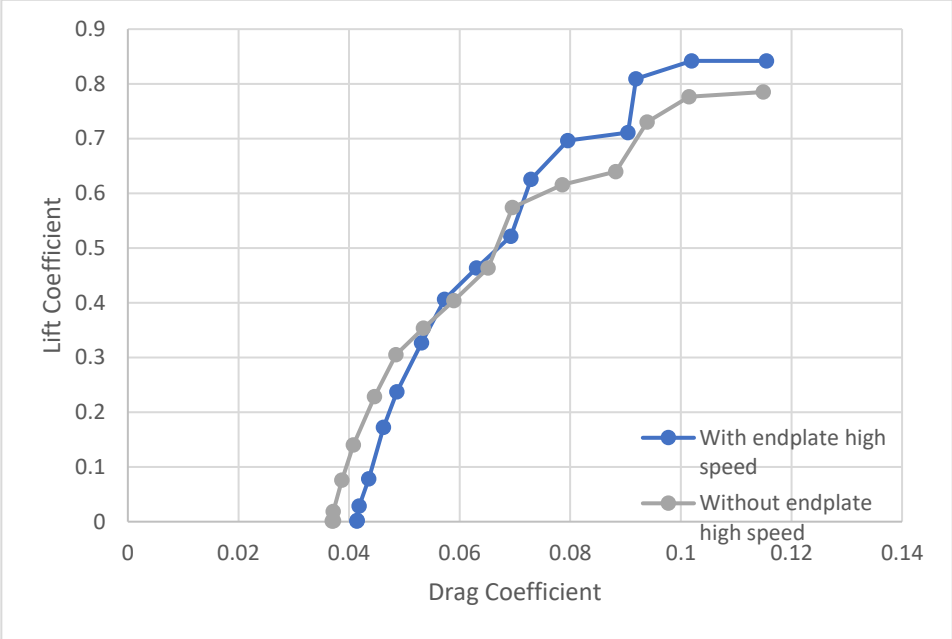

Figure 7: Drag polar for freestream velocity of ~16 m/s with and without endplate (at non-stalling angles of attack)

At non-stalling angles of attack, the effectiveness of the endplate increases as C_d increases. Since C_d increases with angle of attack (Figures 5 and 6), effectiveness of the endplate could be said to increase as α increases at higher speeds.

The same is true even moreso with lower speeds, as one can see in Figure 8.

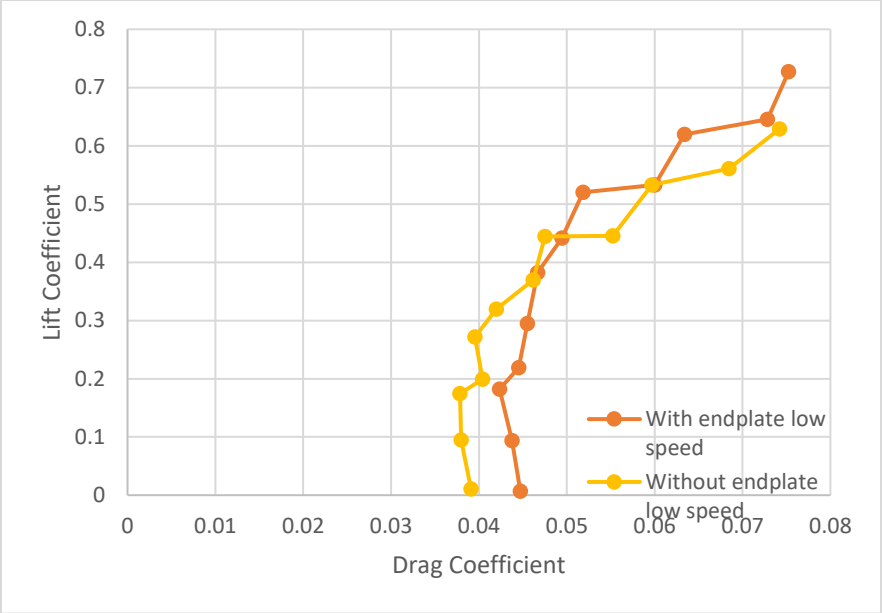

Figure 8: Drag polar for freestream velocity of ~13 m/s with and without endplate (at non-stalling angles of attack)

At increasing C_d (thus increasing α), the endplate seems to increase the C_l to C_d ratio of the wing.

Because of the imbalance of force distribution on the wing, there is a pitching moment in both freestream velocity cases, as shown in Figures 9 and 10.

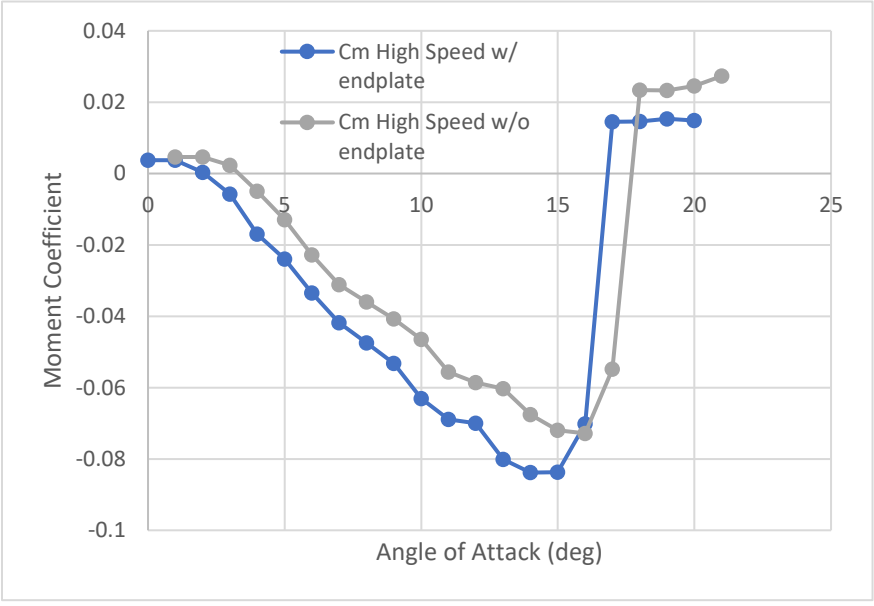

Figure 9: C_m vs. a for freestream velocity of ~16 m/s.

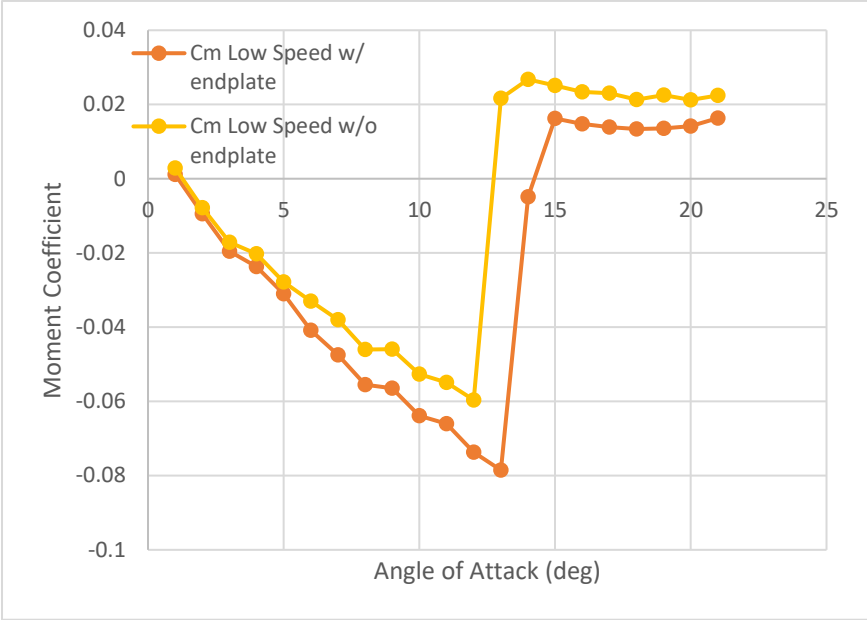

Figure 10: C_m vs. a for freestream velocity of ~13 m/s.

The pitching moment coefficient is stabilizing (negative) until stall, where it becomes positive. This trend makes sense because if the pitching moment were positive before stall occurred, it would reinforce itself and increase the angle of attack, creating a condition where stall occurred faster. With an endplate present, the pitching moment is even more negative. This could mean that with an endplate present, the distribution of forces over a wing is such that the stabilizing moment is stronger, especially with increasing angles of attack.

High vs. Low Freestream Velocity Discussion

Moreso than the inclusion of an endplate, the results show that freestream velocity has a large effect on the C_l vs. a curve. Figures 11 and 12 show that stall occurs much sooner with lower velocities than with higher velocities. (Since stall can be identified from the iconic sudden drop in the C_l vs α curve, it is not necessary to include the C_d vs. α figure to clearly show stall)

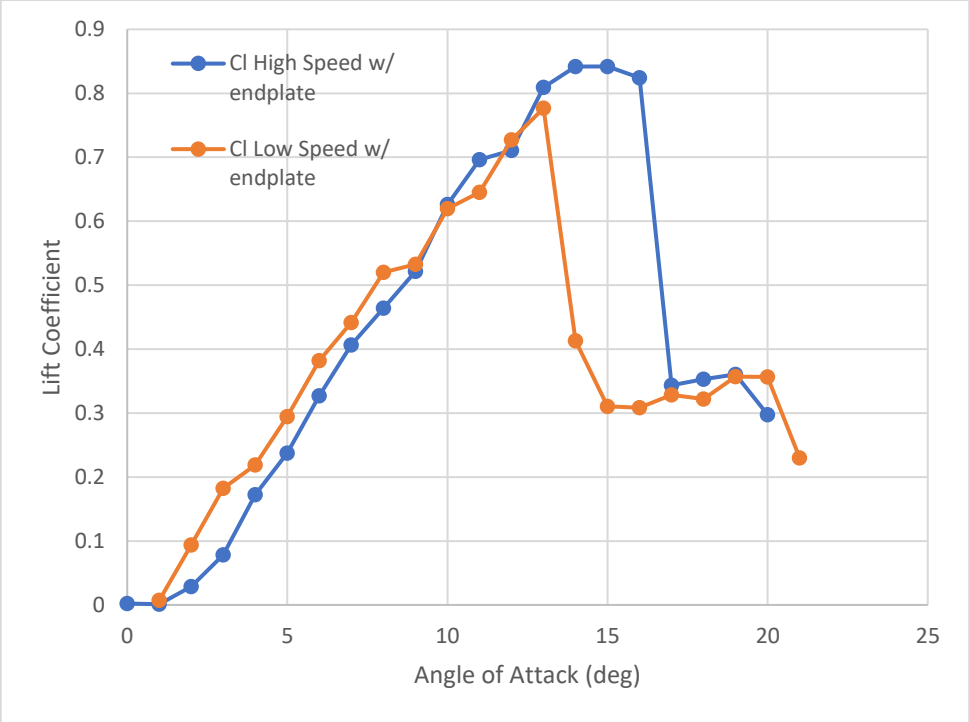

Figure 11: C_l vs α at high speed vs. low speed with endplate

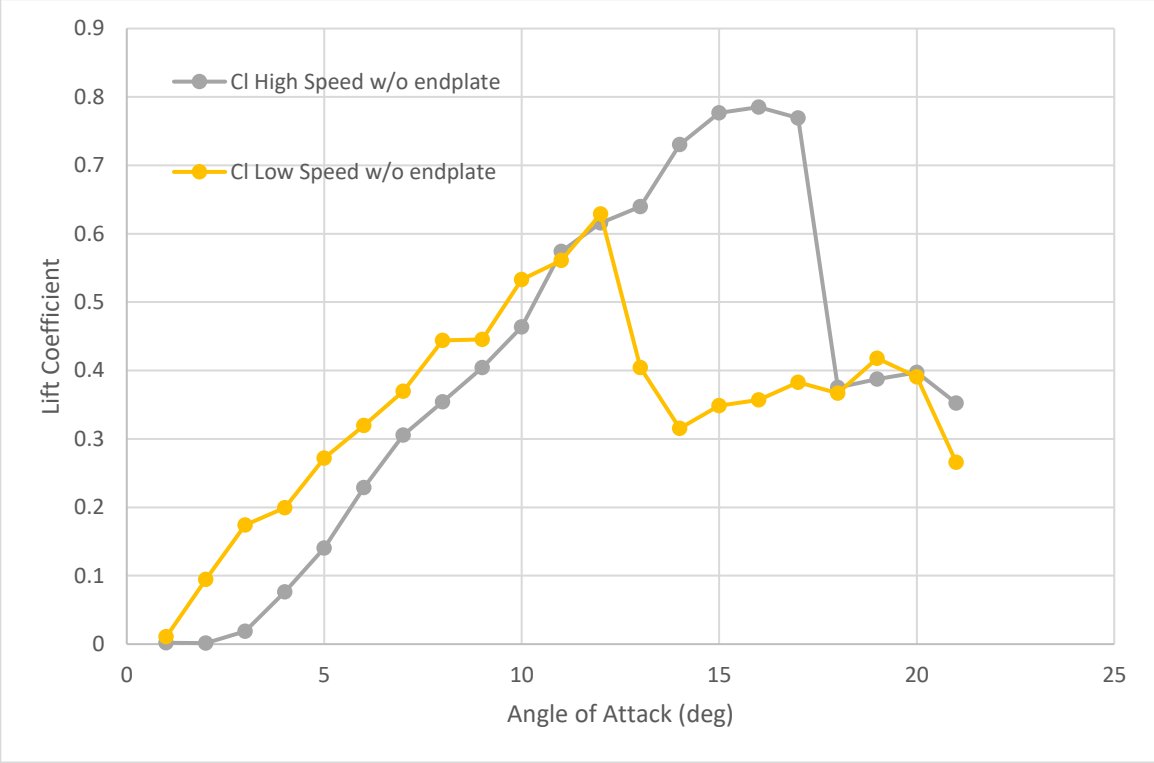

Figure 12: C_l vs. α at high speed vs. low speed without endplate

Theoretically, stall occurs as a result of boundary layer separation. When an airfoil reaches a certain angle of attack, an adverse pressure gradient created by friction effects (the air in the boundary layer needing to speed up quickly) causes the boundary layer velocity profile to go the opposite direction of the freestream velocity, and this causes separation of the boundary layer. Without a boundary layer, there is no effective lift, and thus the wing stalls. When there is more kinetic energy in the flow, the boundary layer is more likely to have more energy. More energy can cause a boundary layer to be turbulent, rather than laminar. Turbulent flow has eddies that mix the freestream air with the boundary layer air – this helps the air speed up from 0 to the freestream velocity, which causes the boundary layer to "stick" to the airfoil longer. The experimental data in Figures 11 and 12 confirms this theory.

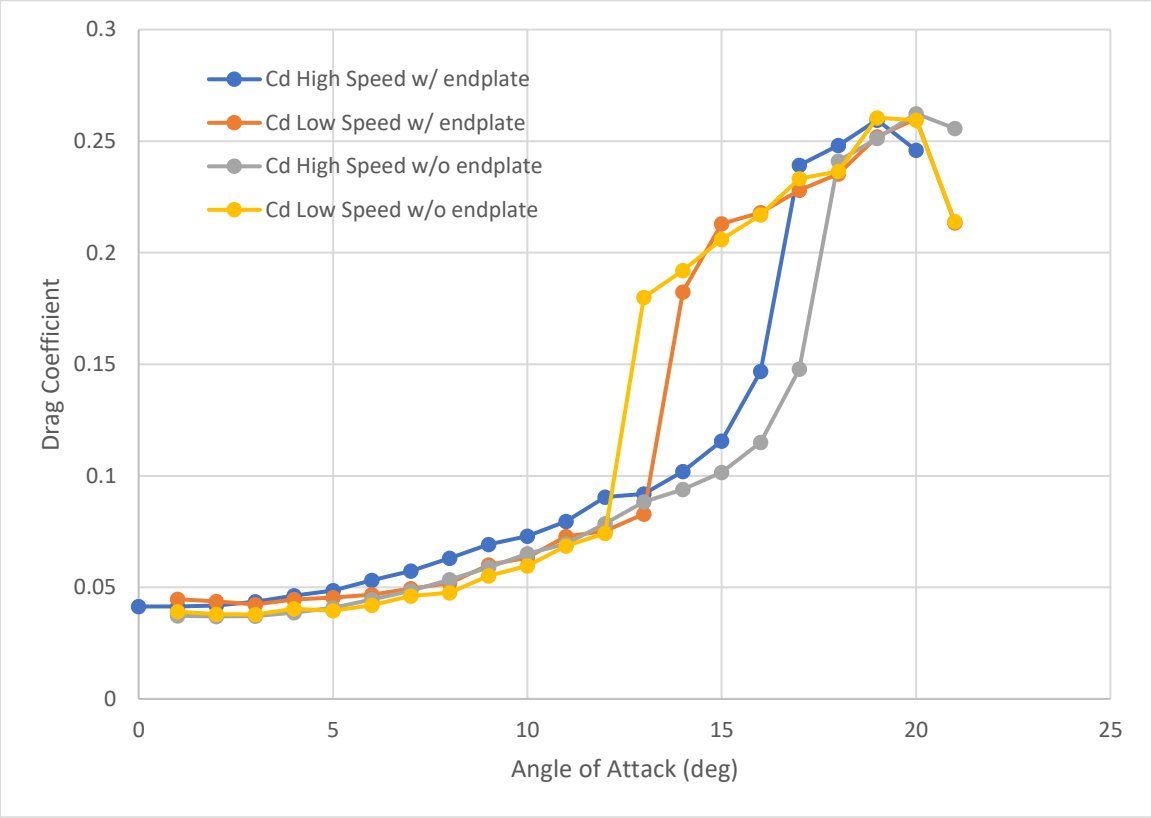

Figure 13: C_d vs. α for all 4 experimental conditions (high speed, low speed, with endplate, without endplate)

Figure 13 shows that the velocity has a remarkable effect on the C_d as well. At lower velocities, stall can be seen at angles of attack of 12 to 13 degrees as opposed to 15 to 16 degrees. Figure 13 corroborates the observations about C_l made while looking at Figures 11 and 12.

Supplemental Questions

(Located in the error analysis section)

Summary and Conclusions

The two parameters studied in this series of experiments were: velocity and endplate. The observations about velocity could be made after calculating the coefficients of lift, drag, and moment and comparing them to angle of attack. Observations about the presence of an endplate on the wing could also be made with plots versus angle of attack, but it was also helpful to analyze the drag polar. Data measurements were taken with those goals in mind and consisted of a few seconds of load cell data and Baratron data for each angle of attack under each parameter of comparison. It was found that under low-speed conditions, stall occurs sooner. This is evidence supportive of the theory that stall occurs due to boundary layer separation. It was also found that an endplate can increase the Lift to Drag ratio at near-stall angles of attack. This could support finite wing theory, and specifically the idea that downwash occurs.

Appendix: Error Analysis

Supplemental Questions

The three instruments used to perform our analyses were the Baratron, the Load Cell, and the FlowKinetics. Since information from the FlowKinetics was only used in order to understand the freestream velocity, the variance of which is talked about further below, the systematic and random errors from the Baratron and Load Cell are going to be treated as more important. The pertinent relations in our uncertainty and error analysis are equations 4, 5, and 6 for C_l, C_d, and C_m. For the sake of brevity, I will only remark on the uncertainty measurements in C_l and C_d for the equation at higher freestream velocity with the endplate. LabView recorded many Fx and Fy measurements for each angle of attack. From those, the standard deviation was calculated and Eqs. 7 and 8 were used to calculate the random uncertainty for F_x abnd F_y.

$$U_{Fx,y\ random} = 1.95\sigma_{\bar{x}} \tag{7}$$

$$\sigma_{\bar{x}} = \frac{s_x}{\sqrt{n}} \tag{8}$$

u is the uncertainty in the F_x or F_y calculations. 1.95 is the factor for 95% confidence level, and $\sigma_{\bar{x}}$ is the standard deviation of the mean, which is represented in Eq. 8. s_x is the standard deviation calculated with MS Excel and n is the number of samples for each angle of attack. The systematic uncertainty for Forces measured by the load cell was taken from the technical manual, which stated that the resolution for both F_x and F_y was 1/160 N. The general uncertainty from the forces was therefore the square root of the sum of the random percent uncertainty squared and the systematic uncertainty given in the manual squared.

$$U_{Fx,y} = \sqrt{U_{Fx,y\ random}{}^2 + \frac{1}{160}{}^2} \tag{9}$$

Because F_x and F_y were used to calculate Lift, the Uncertainty of Lift was calculated using Eq. 10:

$$U_L = \sqrt{\left(\frac{\partial L}{\partial Fx} U_{Fx}\right)^2 + \left(\frac{\partial L}{\partial Fy} U_{Fy}\right)^2} \quad (10)$$

U_{Fx} and U_{Fy} in Eq 10 were calculated from Eq 8 and 9 and Eq 2 was used to find the partial derivative of L with respect to F_x and F_y.

According to the given schematics, the percentage accuracy of the Baratron is 0.05% and there is a resolution of 0.01% of 10 Torr, which is the system's maximum range. Similar to F_x and F_y, the uncertainty for q_∞ was found by taking the square root of the sum of the percent accuracy of the mean value squared and the resolution squared.

$$U_{q\infty} = \sqrt{(0.05\% * P)^2 + 0.001^2} \quad (11)$$

P is the average dynamic pressure in mmHG/Torr measured by the Baratron.

The equation for C_l involves q_∞ and L (likewise the C_d equation involves q_∞ and D) so, the uncertainty for C_l and C_d were calculated using the following two equations:

$$U_{Cl} = \sqrt{\left(\frac{\partial Cl}{\partial L} U_L\right)^2 + \left(\frac{\partial Cl}{\partial q\infty} U_{q\infty}\right)^2} \quad (12)$$

$$U_{Cd} = \sqrt{\left(\frac{\partial Cd}{\partial D} U_D\right)^2 + \left(\frac{\partial Cd}{\partial q\infty} U_{q\infty}\right)^2} \quad (13)$$

Figures 14 and 15 show the C_l and C_d vs α curves plotted with error bars.

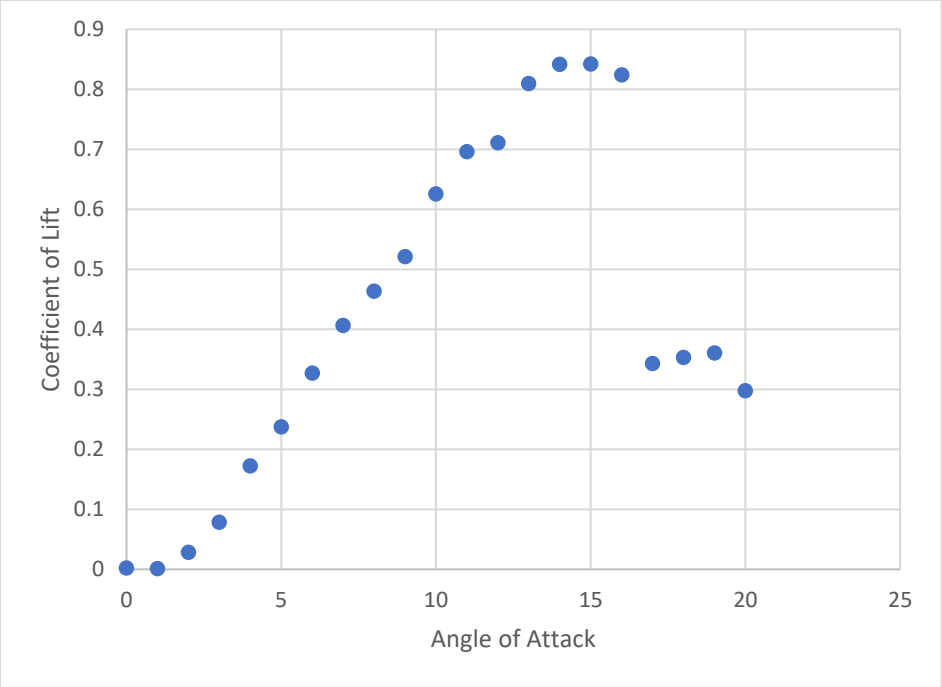

Figure 14: C_l vs α at ~16 m/s with endplate and error bars at 95% confidence intervals

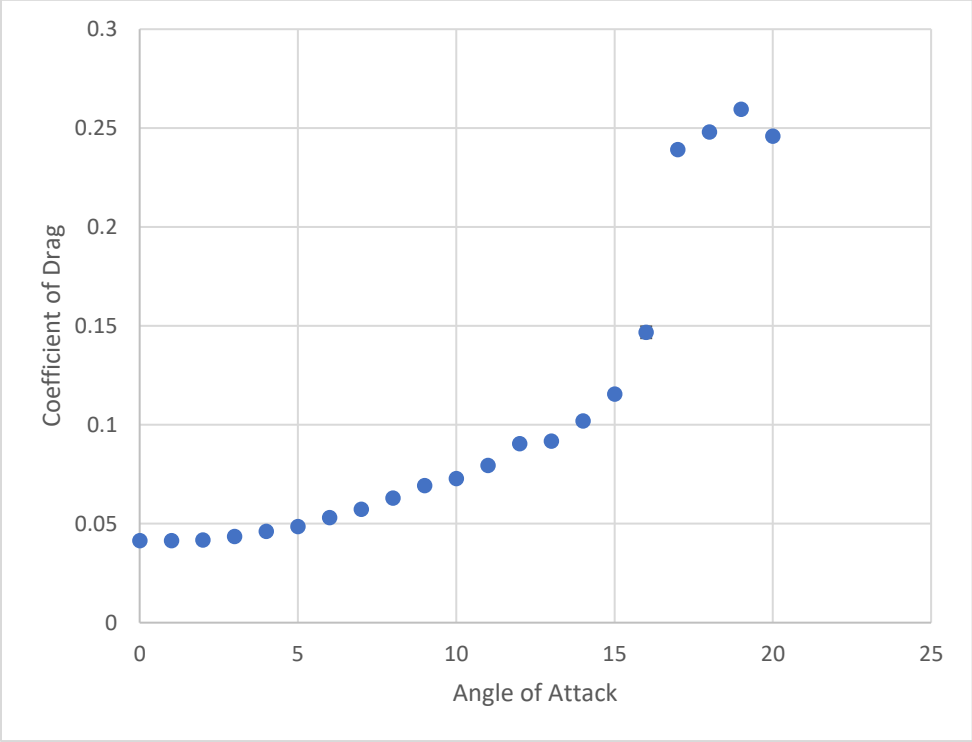

Figure 15: C_d vs α at ~16 m/s with endplate and error bars at 95% confidence intervals.

The error bars in both Figures 14 and 15 are miniscule compared with the scale of the experiment, that is why it is impossible to see them. For a clearer perspective on the contribution to the error to C_l and C_d, I have constructed Figures 16 and 17.

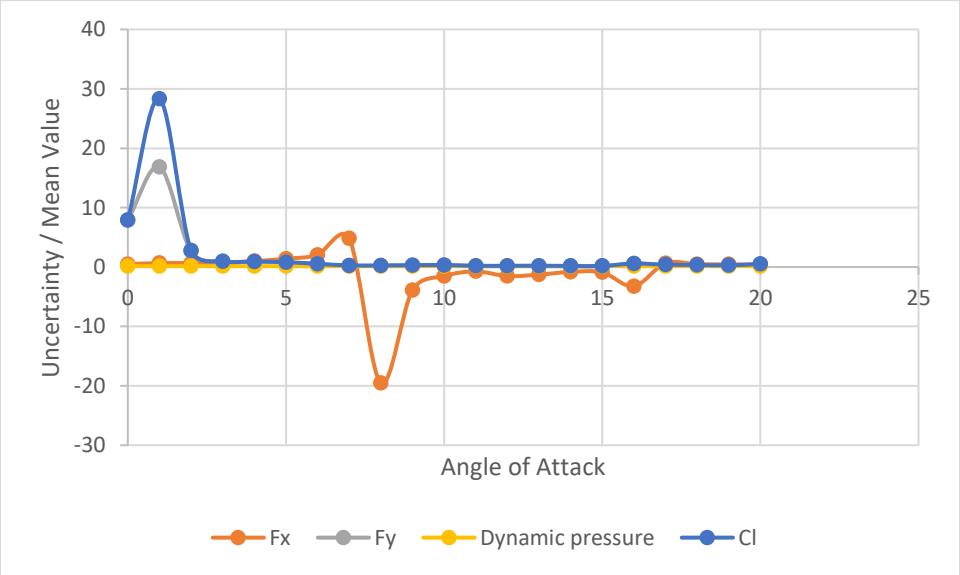

Figure 16: A curve displaying the percent uncertainty for C_l shown against the percent uncertainty value for all the measurements contributing to C_l.

From Figure 16, it is easy to see that fluctuations in uncertainty of F_x do not factor in to the total uncertainty for C_l. However, at lower angles of attack, we can see that a spike in the uncertainty of F_y had a large effect on the uncertainty of C_l. Therefore, for C_l, the largest source of error would be the load cell, specifically in the F_y direction.

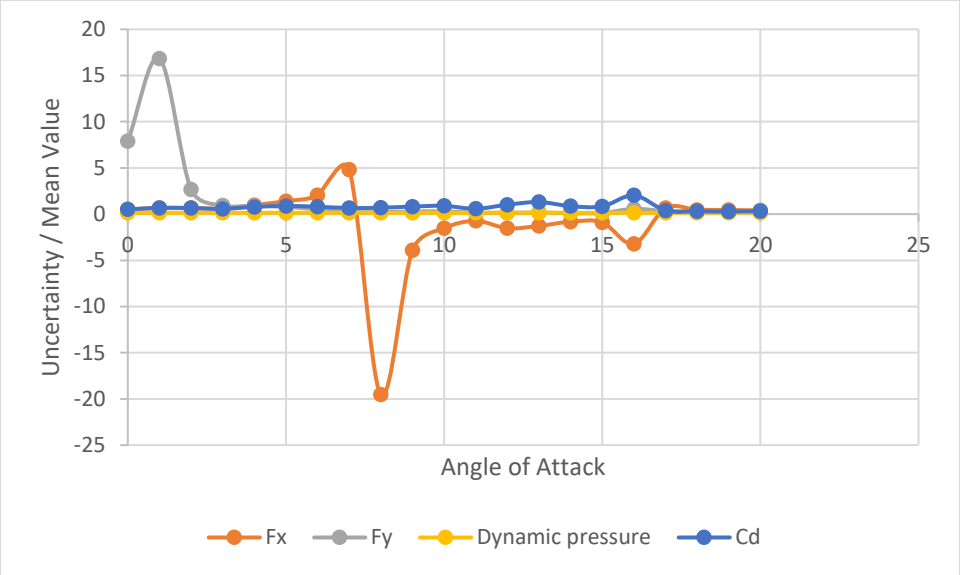

Figure 17: Percent uncertainty for C_d shown against the percent uncertainty values for all measurements contributing to C_d.

In the case of C_d, as Figure 17 shows, it seems that uncertainty in F_x and F_y do not have much of a relationship with uncertainty in C_d. When comparing the contribution of F_y to the uncertainty of C_d however, one can see how at an angle of attack of 16 degrees, F_y is contributes to the little "bump." (Figure 18 below)

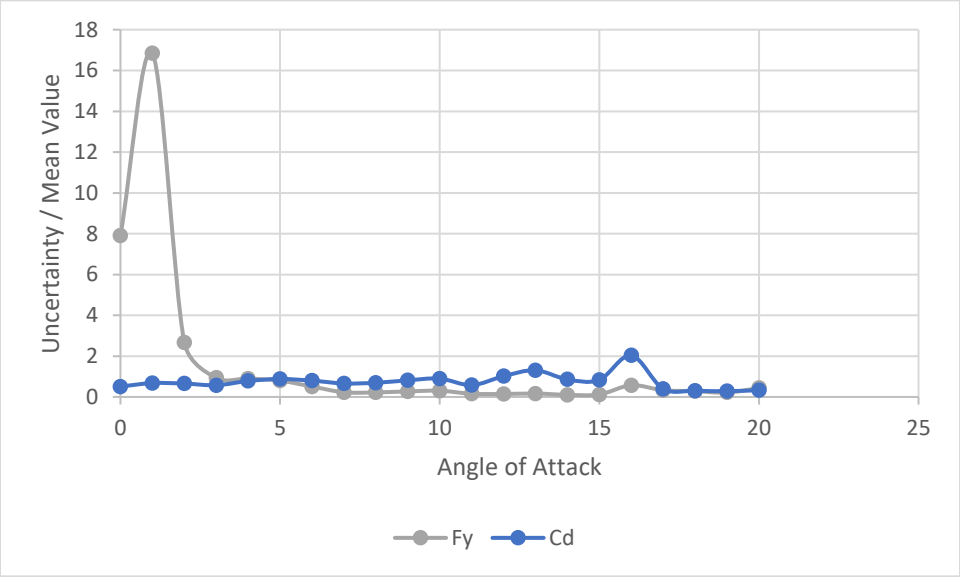

Figure 18: Percent uncertainty of F_y compared to C_d

Again, I conclude that the largest source of error is the load cell. However, because of the method of calculation (using equations 7 and 8) and because the number of samples collected were so numerous (around 4600 for each angle of attack and each experiment), the error with 95% confidence is extremely small.

Even though the error is small, it is worth commenting on what could be causing it. Both the load cell and the Baratron are hooked up with wires. Wiring is not perfect and voltage can fluctuate due to imperfect connections, resistance changes due to temperature variance, or maybe kinks or imperfections in the cables. I did not inspect the cable connections, but I glimpsed them and they seemed old.

Another source for error on the load cell might be the fact that a large assumption on the part of our calculations was that the flow was steady and irrotational. These assumptions are based on the construction of the wind tunnel. The flow was forced through a honeycomb grating in order to get rid of the rotationality, but the honeycomb grid was fairly large (I can estimate about 3 inches across each honeycomb), and so any irrotationality in the flow that was smaller may have remained. The flow also may not have been steady since it was generated by a fan – I can guess that the fan was designed to produce as steady a flow as necessary in order to produce meaningful results, but I cannot be sure since I am not an expert in the flows produced by such turbines. Since there were no tools present by which to monitor the steadiness or rotationality of the flow, it is not useful to guess on this point.

Other Sources of Error

A large systematic error that will not show up in the standard uncertainty analysis is that the velocity of the freestream could not be directly controlled. For the high-speed condition, results are easy to compare and analyze, because the wind tunnel was at its maximum velocity. However, when repeating the experiment at lower freestream velocities, the method of changing the wind tunnel speed was an analog dial that relied on live feedback from LabView. It must be mentioned that the average freestream velocity for the low-speed experiment was not calculated in between experiments, and so when "tuning" the analog dial to the lower speed, we had to rely on our memory to try to turn the dial to where it was. As Table II shows, the low-speed wind condition differed by about 0.5 m/s between experiments. This is a difference larger than 3 percent and makes close analysis difficult, so it may not be worth while to compare the endplate vs. non-endplate results at lower freestream velocities.